Higgs boson decays $h \to MZ$ in the TNMSSM*

Huai-Cong Hu (胡怀聪)† Zhao-Yang Zhang (张兆阳)‡ Ning-Yu Zhu (朱宁宇)§ Hai-Xiang Chen (陈海翔)¶

School of Physical Science and Technology, Guangxi University, Nanning 530004, China

Abstract: We study the SM-like Higgs boson decays $h \to MZ$ in the triplet extended NMSSM (TNMSSM), where M is a vector meson $(\rho, \omega, \phi, J/\psi, \Upsilon)$. Compared to the minimal supersymmetric standard model (MSSM), the TNMSSM includes two new $SU(2)$ triplets with hypercharge ±1 and an SM gauge singlet, which are coupled to each other. The indirect contributions to the $h \to MZ$ decays are produced from the effective $h\gamma Z$ vertex, and they are more important than the direct contributions. The results of this work could encourage a detection on $h \to Z\gamma$ at the future high energy colliders for exploring new physics beyond the SM.

Keywords: supersymmetry, Higgs boson decay

DOI: 10.1088/1674-1137/ad5427

I. INTRODUCTION

Since the Higgs was discovered by the ATLAS and CMS collaborations in 2012 [1, 2], many questions regarding its properties remain unanswered. According to the latest experimental data, the measured mass of the Higgs boson is [3]

$$m_h = 125.25 \pm 0.17 \text{ GeV}.$$

As a new elementary particle, h is largely consistent with the neutral Higgs boson predicted by the standard model (SM). However many questions have been raised that challenge the SM framework.

Weak scale supersymmetry (SUSY) is a promising extension of the SM. It naturally explains why the electroweak (EW) symmetry breaking scale is much smaller than the Planck scale and solves the gauge hierarchy problem [4, 5]. However, the minimum supersymmetric SM (MSSM) cannot fully solve the hierarchy problem. Moreover, it has another problem named "the μ problem". Hence, extensions of the MSSM have been proposed to solve these problems. For example, an extension of the MSSM by adding a (SM) gauge singlet that is coupled to Higgs doublets (the NMSSM) has been proposed to solve the μ problem.

Unfortunately, the NMSSM with all the couplings being perturbative up to the GUT scale also does not really solve the little hierarchy problem [6−9]. If the little hierarchy problem is taken seriously, then one should consider another source of Higgs quadruple coupling, which will not decouple in the large $\tan\beta$ limit [10]. The model that extends the MSSM by adding $SU(2)$ triplets, the triplet extended NMSSM (TMSSM) [11−13], possesses such a Higgs quartic coupling naturally.

The combined advantages of NMSSM and TNMSSM can solve each other's problems [10]. In the TNMSSM, the singlet interactions do not play any important role in raising the physical Higgs mass: one relies on triplets instead of achieving this goal, and hence, one does not face the usual little hierarchy problems of the NMSSM.

This work study the 125 GeV SM-like Higgs boson decay $h \to MZ$ in the framework of TNMSSM, with M representing the mesons ρ, ω, ϕ, J/ψ, and Y. The $h \to MZ$ decay has been shown in [14−20] via the effective vertex $hZ\gamma^*$ and subsequent transition to $\gamma^* \to M$. No $hZ\gamma$ coupling exists at tree level, but it can be contributed by the loop diagram [14]. The first evidence for the $h \to \gamma Z$ process was presented by the ATLAS and CMS collaborations. The obseved signal strength at the 68% confidence level is $\mu = 2.2^{+1.0}_{-0.9}$ for the ATLAS analysis, $\mu = 2.4^{+1.0}_{-0.9}$ for the CMS analysis, and $\mu = 2.2 \pm 0.7$ for their combination [21]. The $h \to \gamma Z$ process has been ob-

Received 2 March 2024; Accepted 4 June 2024; Published online 5 June 2024

* Supported by the National Natural Science Foundation of China (NNSFC) (12075074, 12235008), Natural Science Foundation of Guangxi Autonomous Region (2022GXNSFDA035068), Hebei Natural Science Foundation (A2022201017, A2023201041), the youth top-notch talent support program of the Hebei Province

† E-mail: huaiconghu@163.com

‡ E-mail: 1311274306@qq.com

§ E-mail: hnzhuny@163.com

¶ E-mail: haixchen@hotmail.com

served, and the results are shifted from the SM. This presupposes the existence of a new physics, whose contribution to the process may be able to explain the deviations between the observed decays and SM predictions, and thus the associated decay process deserves to be investigated. This coupling is important for probing a new physics. In the TNMSSM, additional coupling exists of the Higgs boson to additional charged scalars and charged fermions. They contribute to the $hZ\gamma$ coupling through loop diagrams.

This paper is organized as follows. We briefly present the main ingredients of the TNMSSM in Sec. II. We present the Higgs boson decay $h \to Z\gamma$ and $h \to MZ$ formulas in Sec. III. We show the input parameters and numerical results in Sec. IV. In the last section, we present the discussion and conclusion. Finally, some related formulas are included in the Appendix.

II. THE TRIPLET EXTENDED NMSSM (TNMSSM)

Compared to the MSSM, the TNMSSM includes two new $SU(2)_L$ triplet superfields T, $\bar{T}$ with hypercharge ±1 and an SM gauge singlet superfield $\hat{s}$, which are coupled to each other.

The superpotential of the TNMSSM can be written as follows:

$$W = -Y_d \hat{d}\hat{q}\hat{H}_d - Y_e \hat{e}\hat{l}\hat{H}_d + \chi_d \hat{H}_d \hat{T} \hat{H}_d + \lambda \hat{H}_u \hat{H}_d \hat{s} + \chi_t \hat{H}_u \hat{\bar{T}} \hat{H}_u + \frac{1}{3}\kappa \hat{s}^3 + \Lambda_T \hat{s}\hat{\bar{T}}\hat{T} + Y_u \hat{u}\hat{q}\hat{H}_u .$$

Here, the triplet superfields with hypercharge $Y = \pm 1$ are defined as

$$T \equiv T^a \sigma^a = \begin{pmatrix} T^+/\sqrt{2} & -T^{++} \\ T^0 & -T^+/\sqrt{2} \end{pmatrix}$$

$$\bar{T} \equiv \bar{T}^a \sigma^a = \begin{pmatrix} \bar{T}^-/\sqrt{2} & -\bar{T}^0 \\ \bar{T}^- & -\bar{T}^-/\sqrt{2} \end{pmatrix}$$

The soft SUSY breaking terms are as follows:

$$\begin{aligned} -\mathcal{L}_{\text{soft}} = {} & \frac{1}{2}(M_1\lambda_1\lambda_1 + M_2\lambda_2\lambda_2 + M_3\lambda_3\lambda_3 + h.c.) + m_{Hu}^2|H_u|^2 + m_{H_d}^2|H_d|^2 + m_{\bar{T}}^2 Tr(\bar{T}^\dagger \bar{T}) + m_T^2 Tr(T^\dagger T) + m_S^2|S|^2 + m_{\tilde{Q}}^2|\tilde{Q}|^2 \\ & + m_{\tilde{u}}^2|\tilde{u}_R|^2 + m_{\tilde{d}}^2|\tilde{d}_R|^2 + m_{\tilde{l}}^2|\tilde{l}|^2 + m_{\tilde{e}}^2|\tilde{e}_R|^2 + (T_{\Lambda T} tr(T\bar{T})S + T_{\chi d} H_d \cdot T H_d + T_{\chi_t} H_u \cdot \bar{T} H_u + \frac{T_\kappa}{3} S^3 + T_\lambda H_u \cdot H_d S \\ & + T_d H_d \cdot \tilde{Q} d^* - T_u H_u \cdot \tilde{Q} u^* + T_e H_d \cdot L e^* + \text{h.c.}), \end{aligned} \tag{1}$$

where the respective definitions of the products between the two $SU(2)_L$ doublets and between the $SU(2)_L$ doublets and $SU(2)_L$ triplet are given as follows:

$$\begin{aligned} H_u \cdot H_d &= H_u^+ H_d^- H_u^0 H_d^0, \\ H_u \cdot \bar{T} H_u &= \sqrt{2} H_u^0 H_u^+ \bar{T}^- (H_u^0)^2 \bar{T}^0 - (H_u^+)^2 \bar{T}^-, \\ H_d \cdot T H_d &= \sqrt{2} H_d^0 H_d^- T^+ - (H_d^0)^2 T^0 - (H_d^-)^2 T^{++}. \end{aligned}$$

Once the electroweak symmetry is spontaneously broken, the neutral scalar fields can be defined as

$$\begin{aligned} \langle H_u^0 \rangle &= \frac{v_u + \phi_u + i\sigma_u}{\sqrt{2}}, \qquad \langle H_d^0 \rangle = \frac{v_d + \phi_d + i\sigma_d}{\sqrt{2}}, \\ \langle T^0 \rangle &= \frac{v_T + \phi_T + i\sigma_T}{\sqrt{2}}, \qquad \langle \bar{T}^0 \rangle = \frac{\bar{v}_T + \phi_{\bar{T}} + i\sigma_{\bar{T}}}{\sqrt{2}}, \\ \langle S \rangle &= \frac{v_s + \phi_s + i\sigma_s}{\sqrt{2}}. \end{aligned}$$

We define the ratio v_u to v_d as $\tan\beta = \dfrac{v_u}{v_d}$, and the ratio v_T to $v_{\bar{T}}$ as $\tan\beta' = \dfrac{v_T}{v_{\bar{T}}}$.

Because we introduce a single state and two triplet states, we have five minimization equations, including the usual upper and lower Higgs. In general, the vacuum expectation value of the triplet states must be small to avoid large ρ-parameter corrections [10].

In the basis $(H_d^-, H_u^{+,*}, \bar{T}^-, T^{+,*})$ and $(H_d^{-,*}, H_u^+, \bar{T}^{-,*}, T^+)$, the definition of the mass squared matrix for a charged Higgs is given by

$$m_{H^-}^2 = \begin{pmatrix} m_{H_d^-, H_d^{-,*}} & m^*_{H_u^{+,*}, H_d^{-,*}} & m^*_{\bar{T}^-, H_d^{-,*}} & m^*_{T^{+,*}, H_d^{-,*}} \\ m_{H_d^-, H_u^+} & m_{H_u^{+,*}, H_u^+} & m^*_{\bar{T}^-, H_u^+} & m^*_{T^{+,*}, H_u^+} \\ m_{H_d^-, \bar{T}^{-,*}} & m_{H_u^{+,*}\bar{T}^{-,*}} & m_{\bar{T}^-\bar{T}^{-,*}} & m^*_{T^{+,*}\bar{T}^{-,*}} \\ m_{H_d^-, T^+} & m_{H_u^{+,*}T^+} & m_{\bar{T}^-T^+} & m_{T^{+,*}T^+} \end{pmatrix} \tag{2}$$

where

$$m_{H_d^-, H_d^{-,*}} = \frac{1}{2}v_s^2|\lambda|^2 + \frac{1}{8}\left[g_1^2(2v_{\bar{T}}^2 - 2v_T^2 - v_u^2 + v_d^2) + g_2^2(-2v_{\bar{T}}^2 + 2v_T^2 + v_d^2 + v_u^2)\right] + v_d^2|\chi_d|^2 + m_{H_d}^2,$$

$$
\begin{aligned}
m_{H_d^-,H_u^+} &= \frac{1}{2}\left[\lambda(-v_d v_u\lambda^* + v_s^2\kappa^* - v_T v_{\bar{T}}\Lambda_T^*) + \sqrt{2}v_s T_\lambda\right] + \frac{1}{4}g_2^2 v_d v_u,\\
m_{H_u^{+,*},H_u^+} &= \frac{1}{2}v_s^2|\lambda|^2 + \frac{1}{8}\left[(g_1^2+g_2^2)v_u^2 - (-g_2^2+g_1^2)(2v_{\bar{T}}^2 - 2v_T^2 + v_d^2)\right] + v_u^2|\chi_t|^2 + m_{H_u}^2,\\
m_{H_d^-,\bar{T}^{-,*}} &= \frac{1}{2\sqrt{2}}g_2^2 v_d v_{\bar{T}} - \frac{1}{\sqrt{2}}v_s(v_d\chi_d\Lambda_T^* + v_u\lambda\chi_t^*),\\
m_{H_u^{+,*}\bar{T}^{-,*}} &= \frac{1}{2\sqrt{2}}g_2^2 v_{\bar{T}} v_u + \frac{1}{\sqrt{2}}(-2v_{\bar{T}}v_u\chi_t + v_d v_s\lambda)\chi_t^* - v_u T_{\chi,t^*},\\
m_{\bar{T}^-\bar{T}^{-,*}} &= \frac{1}{2}v_s^2|\Lambda_T|^2 + \frac{1}{4}\left[2g_2^2 v_{\bar{T}}^2 + (g_1^2 2v_{\bar{T}}^2 - 2v_T^2 - v_u^2 + v_d^2)\right] + v_u^2|\chi_t|^2 + m_{\bar{T}}^2,\\
m_{H_d^-,T^+} &= \frac{1}{2\sqrt{2}}g_2^2 v_d v_T + \frac{1}{\sqrt{2}}v_s v_u\chi_d\lambda^* - v_d(\sqrt{2}v_T|\chi_d|^2 + T_{\chi d}),\\
m_{H_u^{+,*}T^+} &= \frac{1}{2\sqrt{2}}g_2^2 v_d v_u - \frac{1}{\sqrt{2}}v_s(\Lambda_T v_u\chi_t^* + v_d\chi_d\lambda^*),\\
m_{\bar{T}^-T^+} &= \frac{1}{2}g_2^2 v_T v_{\bar{T}} + \frac{1}{2}\left[\Lambda_T(-v_d v_u\lambda^* + v_s^2\kappa^* - v_T v_{\bar{T}}\Lambda_T^*) + \sqrt{2}v_s T_{\Lambda_T}\right],\\
m_{T^{+,*}T^+} &= \frac{1}{2}v_s|\Lambda_T|^2 + \frac{1}{4}\left[2g_2^2 v_T^2 + g_1(-2v_{\bar{T}}^2 + 2v_T^2 - v_d^2 + v_u^2)\right] + v_d^2|\chi_d|^2 + m_T^2.
\end{aligned}
$$

This matrix is diagonalized by Z^+:

$$Z^+ m_{H^-}^2 Z^{+,\dagger} = m_{2,H^-}^{\rm dia}$$

with

$$H_d^- = \sum_j Z_{j1}^+ H_j^-,\quad H_u^+ = \sum_j Z_{j2}^+ H_j^+,$$

$$T^- = \sum_j Z_{j3}^+ H_j^-,\quad T^+ = \sum_j Z_{j4}^+ H_j^+.$$

The mass of the SM-like Higgs boson in the TNMSSM can be written as

$$m_h = \sqrt{(m_{h_1}^0)^2 + \Delta m_h^2}, \tag{3}$$

where $m_{h_1}^0$ is the lightest tree-level Higgs boson mass, and Δm_h^2 is the radiative correction. The two-loop leading-log radiative corrections can be given as

$$
\begin{aligned}
\Delta m_h^2 = \frac{3m_t^4}{4\pi^2 v^2}\Bigg[&\left(\tilde{t} + \frac{1}{2}\tilde{X}_t\right) + \frac{1}{16\pi^2}\left(\frac{3m_t^2}{2v^2} - 32\pi\alpha_3\right)\\
&\times\left(\tilde{t}^2 + \tilde{X}_t\tilde{t}\right)\Bigg],
\end{aligned}
\tag{4}
$$

$$\tilde{t} = \log\frac{M_S^2}{m_t^2},\qquad \tilde{X}_t = \frac{2\tilde{A}_t^2}{M_S^2}\left(1 - \frac{\tilde{A}_t^2}{12M_S^2}\right), \tag{5}$$

where α_3 is the running strong coupling constant. $M_S = \sqrt{m_{\tilde{t}_1}m_{\tilde{t}_2}}$, where $m_{\tilde{t}_{1,2}}$ are the stop masses. $\tilde{A}_t = A_t - \mu\cot\beta$, with $A_t = T_{u,33}/Y_{u,33}$.

III. ANALYTICAL FORMULA

In this section, we discuss the Higgs boson decay processes $h\to Z\gamma$ and $h\to MZ$. The dominating Feynman diagrams for $h\to MZ$ are shown in Fig. 1. The first two diagrams in Fig. 1 are the direct contributions, and the last two diagrams represent the indirect contributions. For the indirect contribution, there is a process $h\to Z\gamma^*\to MZ$, where γ^* is off-shell and changes into the final state meson.

There is no contribution to $hZ\gamma$ coupling at the tree level in the TNMMSM, but it can be created by loop diagrams. The $h\to Z\gamma^*$ process can be used to probe for a new physics. Thus, we will focus on discussing $h\to Z\gamma^*$. In the TNMSSM, the non-standard $h^0\gamma Z$ vertex should be taken into account. The effective Lagrangian for $h\gamma Z$ is written as

$$\mathcal{L}_{eff} = \frac{\alpha}{4\pi\upsilon}\left(\frac{2C_{\gamma Z}}{s_W c_W}hF_{\mu\nu}Z^{\mu\nu} - \frac{2\tilde{C}_{\gamma Z}}{s_W c_W}hF_{\mu\nu}\tilde{Z}^{\mu\nu}\right), \tag{6}$$

with $s_W = \sin\theta_W, c_W = \cos\theta_W$. The decay width of $h\to Z\gamma$ deduced by the effective Lagrangian defined in Eq. (6) is

$$\Gamma(h\to Z\gamma) = \frac{\alpha^2 m_{h^0}^3}{32\pi^3\upsilon^2 s_W^2 c_W^2}\left(1 - \frac{m_Z^2}{m_{h^0}^2}\right)^3(|C_{\gamma Z}|^2 + |\tilde{C}_{\gamma Z}|^2). \tag{7}$$

The loop diagrams make additional contributions to $h\to MZ$ decays in the new physics. The decay width of $h\to MZ$ is given by

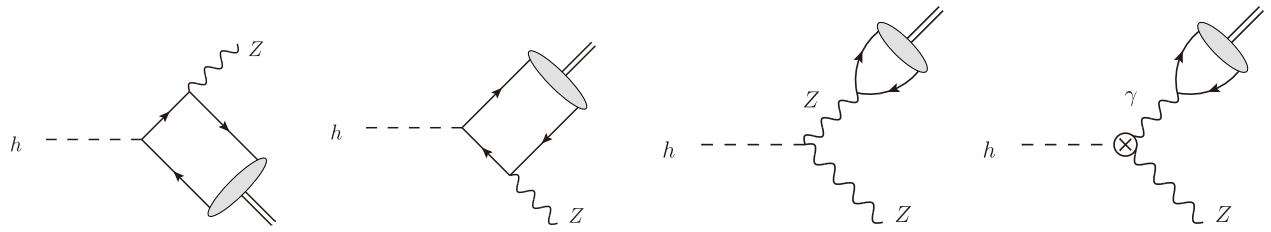

Fig. 1. Diagrams contributing to the decay $h \to MZ$. The crossed circle in the last graph represents the effective vertex $h \to Z\gamma^*$ from the one loop diagrams.

$$\Gamma(h \to MZ) = \frac{m_{h^0}^3}{4\pi v^4}\lambda^{1/2}(1, r_Z, r_M)(1 - r_Z - r_M)^2 \times \left[\left|F_{\parallel}^{MZ}\right|^2 + \frac{8 r_M r_Z}{(1 - r_Z - r_M)^2}\left(\left|F_{\perp}^{MZ}\right|^2 + \left|\tilde{F}_{\perp}^{MZ}\right|^2\right)\right], \quad (8)$$

with $\lambda(x,y,z) = (x-y-z)^2 - 4yz, r_Z = \frac{m_Z^2}{m_h^2}$. $r_M = \frac{m_M^2}{m_h^2}$, and m_M is the mass of a vector meson. $F_{\parallel}^{MZ}$ and $F_{\perp}^{MZ}$ represent the *CP*-even longitudinal and transverse form factors, respectively. $\tilde{F}_{\perp}^{MZ}$ represents the *CP*-odd transverse form factors. For the vector mesons considered in this work, the mass ratio r_M is very small, but it can make significant contributions to the transverse polarization states. To obtain better results, we maintain it in our study.

In Eq. (8), $F_{\parallel}^{MZ}, F_{\perp}^{MZ}$, and $\tilde{F}_{\perp}^{MZ}$ could be divided into direct and indirect parts. The indirect contributions are as follows:

$$F_{\parallel\text{indirect}}^{MZ} = \frac{\kappa_Z}{1 - r_M/r_Z}\sum_q f_M^q v_q + C_{\gamma Z}\frac{\alpha_s(m_M)}{4\pi} \times \frac{4 r_Z}{1 - r_Z - r_M}\sum_q f_M^q Q_q, \quad (9)$$

$$F_{\perp\text{indirect}}^{MZ} = \frac{\kappa_Z}{1 - r_M/r_Z}\sum_q f_M^q v_q + C_{\gamma Z}\frac{\alpha_s(m_M)}{4\pi} \times \frac{1 - r_Z - r_M}{r_M}\sum_q f_M^q Q_q, \quad (10)$$

$$\tilde{F}_{\perp\text{indirect}}^{MZ} = \tilde{C}_{\gamma Z}\frac{\alpha_s(m_M)}{4\pi}\frac{\lambda^{1/2}(1, r_Z, r_M)}{r_M}\sum_q f_M^q Q_q, \quad (11)$$

where $v_q = \frac{T_3^q}{2} - Q_q \sin^2\theta_W$ represents the vector couplings of the Z boson to the quark q. κ_Z is the ratio of the coupling of the SM-like Higgs boson to Z boson to the corresponding SM value. α_s is the strong coupling constant. The flavor-specific decay constants f_M^q are defined by

$$\langle M(k,\varepsilon)|\bar{q}\gamma^\mu q|0\rangle = -\mathrm{i} f_M^q m_M \varepsilon^{*\mu}, \quad q = u, d, s\ldots \quad (12)$$

The calculations can be simplified by the following relationship:

$$\sum_q f_M^q Q_q = f_M Q_M, \quad \sum_q f_M^q v_q = f_M v_M. \quad (13)$$

The vector meson decay constants f_M, Q_M, v_M are listed in Table 1.

The concrete forms of $C_{\gamma Z}$ and $\tilde{C}_{\gamma Z}$ in Eqs. (9)–(11) can be written as [16, 17, 22]

$$C_{\gamma Z} = C_{\gamma Z}^{\rm SM} + C_{\gamma Z}^{\rm NP}, \qquad \tilde{C}_{\gamma Z} = \tilde{C}_{\gamma Z}^{\rm SM} + \tilde{C}_{\gamma Z}^{\rm NP}.$$
$$C_{\gamma Z}^{\rm SM} = \sum_q \frac{2N_c Q_q v_q}{3} A_f(\tau_q, r_Z) + \sum_l \frac{2 Q_l v_l}{3} A_f(\tau_l, r_Z) - \frac{1}{2} A_W^{\gamma Z}(\tau_W, r_Z),$$
$$\tilde{C}_{\gamma Z}^{\rm SM} = \sum_q \tilde{\kappa}_q N_c Q_q v_q B_f(\tau_q, r_Z) + \sum_l \tilde{\kappa}_l Q_l v_l B_f(\tau_l, r_Z), \quad (14)$$

where $\tau_i = \frac{4m_i^2}{m_h^2}$, v_l are the vector couplings of the Z boson to the leptons, and Q_l represents the charge of leptons. $C_{\gamma Z}^{\rm SM}$ and $\tilde{C}_{\gamma Z}^{\rm SM}$ represent the SM contributions to $h \to Z\gamma$. $\tilde{\kappa}_q$ and $\tilde{\kappa}_l$ represent the effective Higgs couplings to the quarks and leptons, respectively. A_f, B_f, and $A_W^{\gamma Z}$ are loop functions that can be found in Refs. [18, 23]. The numerical values of $C_{\gamma Z}^{\rm SM}$ and $\tilde{C}_{\gamma Z}^{\rm SM}$ are taken as $C_{\gamma Z}^{\rm SM} \sim -2.395 + 0.001\mathrm{i}$, $\tilde{C}_{\gamma Z}^{\rm SM} \sim 0$ in Ref. [16].

In the TNMSSM, the one loop diagrams contributing to $h \to \gamma Z$ are shown in Fig. 2, where F represents the charged Fermions and S represents the charged scalars. The new contributions to $C_{\gamma Z}$ originate from the exchanged particles: charginos, sleptons, squarks, and charged Higgs.

The *CP*-odd coupling $\widetilde{C}_{\gamma Z}$ is 0 in the SM. In the TNMSSM, the $h\gamma Z$ coupling can be written as $\bar{F}_1 i(A + B\gamma^5)F_2 h$, where A is the *CP*-even part and B is the *CP*-odd part [16, 17]. For the interaction $\bar{F}_1 i(C^R P_R + C^L P_L)F_2 h$ with $P_L = \frac{1-\gamma_5}{2}$ and $P_R = \frac{1+\gamma_5}{2}$, the *CP*-even part is $A = \frac{1}{2}(C^L + C^R)$ and the *CP*-odd part is $B =$

Table 1. Mesons decay constants f_M, Q_M, v_M used in the numerical analysis, where $f_M^{\perp}$ and $f_M^{q\perp}$ represent the transverse decay constants and flavor-specific transverse decay constants, respectively.

Vector meson	ω	ρ	ϕ	J/ψ	Y
m_M/GeV	0.782	0.77	1.02	3.097	9.46
f_M/GeV	0.194	0.216	0.223	0.403	0.684
v_M	$-\frac{\sin^2\theta_W}{3\sqrt{2}}$	$\frac{1}{\sqrt{2}}(\frac{1}{2}-\sin^2\theta_W)$	$-\frac{1}{4}+\frac{\sin^2\theta_W}{3}$	$\frac{1}{4}-\frac{2\sin^2\theta_W}{3}$	$-\frac{1}{4}+\frac{\sin^2\theta_W}{3}$
Q_M	$\frac{1}{3\sqrt{2}}$	$\frac{1}{\sqrt{2}}$	$-\frac{1}{3}$	$\frac{2}{3}$	$-\frac{1}{3}$
$f_M^{\perp}/f_M=f_M^{q\perp}/f_M^q$	0.71	0.72	0.76	0.91	1.09

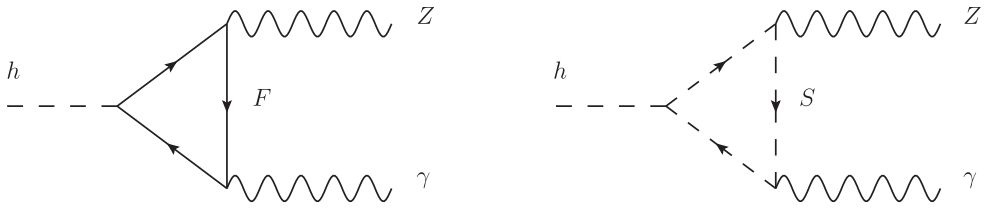

Fig. 2. One loop diagrams for $h\to\gamma Z$ in the TNMSSM, with $F=\chi^{\pm},\chi^{\pm\pm}$ denoting the charged fermions and $S=\tilde{u}_i^{+},\tilde{d}_i^{-},S_\alpha^{\pm},S_\alpha^{\pm\pm}$ denoting the squarks and charged scalars.

$\frac{1}{2}(C^R-C^L)$. In the TNMSSM,

$$C^L_{hS^+S^-}=C^R_{hS^+S^-},\ C^L_{hS^{++}S^-}=C^R_{hS^{++}S^-},\ C^L_{h\tilde{f}\tilde{f}}=C^R_{h\tilde{f}\tilde{f}},$$
$$C^L_{h\chi^+\chi^-}=C^R_{h\chi^+\chi^-},\ C^L_{h\chi^{++}\chi^-}=C^R_{h\chi^{++}\chi^-}$$

and only $C^L_{Z\chi^+\chi^-}\neq C^R_{Z\chi^+\chi^-}$ or $C^L_{Z\chi^{++}\chi^-}\neq C^R_{Z\chi^{++}\chi^-}$. However, $C^L_{Z\chi^+\chi^-}+C^R_{Z\chi^+\chi^-}\gg C^R_{Z\chi^+\chi^-}-C^L_{Z\chi^+\chi^-}$, $C^L_{Z\chi^{++}\chi^-}+C^R_{Z\chi^{++}\chi^-}\gg C^R_{Z\chi^{++}\chi^-}-C^L_{Z\chi^{++}\chi^-}$. Thus, we can neglect the CP-odd coupling $C_{\gamma Z}^{NP}$ in the TNMSSM. The expression of CP-even coupling $C_{\gamma Z}^{NP}$ in the TNMSSM is

$$\begin{aligned}C_{\gamma Z}^{NP}=\frac{c_w}{2}\Big[&\sum_{S^{\pm}}\left(2c_w^2-1\right)g_{hS^+S^-}(m_Z^2/m_{S^{\pm}}^2)A_0[x_{S^{\pm}},\lambda_{S^{\pm}}]\\&+\sum_{S^{\pm\pm}}\left(2c_w^2-1\right)g_{hS^{++}S^-}(m_Z^2/m_{S^{\pm\pm}}^2)A_0[x_{S^{\pm\pm}},\lambda_{S^{\pm\pm}}]\\&+\sum_{\tilde{f}}N_cQ_{\tilde{f}}\hat{v}_{\tilde{f}}g_{h\tilde{f}\tilde{f}}(m_Z^2/m_{\tilde{f}}^2)A_0[x_{\tilde{f}},\lambda_{\tilde{f}}]\\&+\sum_{\chi^{\pm};m,n=L,R}g^m_{h\chi^{\pm}\chi^{\mp}}g^n_{Z\chi^{\pm}\chi^{\mp}}(2m_W/m_{\chi^{\pm}})A_{1/2}[x_{\chi^{\pm}},\lambda_{\chi^{\pm}}]\\&+\sum_{\chi^{\pm\pm};m,n=L,R}g^m_{h\chi^{\pm\pm}\chi^{\mp\mp}}g^n_{Z\chi^{\pm\pm}\chi^{\mp\mp}}(2m_W/m_{\chi^{\pm\pm}})A_{1/2}[x_{\chi^{\pm}\pm},\lambda_{\chi^{\pm}\pm}]\Big]\end{aligned}\tag{15}$$

where $x_i=4m_i^2/m_h^2$, $\lambda_i=4m_i^2/m_Z^2$, $\hat{v}_{\tilde{f}_1}=(T_3^f\cos^2\theta_f-Q_fs_w^2)/c_w$, and $\hat{v}_{\tilde{f}_2}=(T_3^f\sin^2\theta_f-Q_fs_w^2)/c_w$. $\hat{v}_{\tilde{f}_1}$ and $\hat{v}_{\tilde{f}_2}$ represent up and down-quark sectors. T_3^f is the weak isospin of fermion f, θ_f is the mixing angle of sfermions $\tilde{f}_{1,2}$. The functions A_0, $A_{1/2}$ can be found in [23, 24]. The concrete expressions of couplings are as follows:

$$g_{hS^+S^-}=-\frac{v}{2m_Z^2}C^{L,R}_{hS^+S^-},\quad g_{hS^{++}S^-}=-\frac{v}{2m_Z^2}C^{L,R}_{hS^{++}S^-}$$
$$g_{h\tilde{f}\tilde{f}}=-\frac{v}{2m_Z^2}C^{L,R}_{h\tilde{f}\tilde{f}},\quad g^{L,R}_{h\chi^{\pm}\chi^{\mp}}=-\frac{1}{e}C^{L,R}_{h\chi^{\pm}\chi^{\mp}}$$
$$g^{L,R}_{Z\chi^{\pm}\chi^{\mp}}=-\frac{1}{e}C^{L,R}_{Z\chi^{\pm}\chi^{\mp}},\quad g^{L,R}_{h\chi^{\pm\pm}\chi^{\mp\mp}}=-\frac{1}{e}C^{L,R}_{h\chi^{\pm\pm}\chi^{\mp\mp}}$$
$$g^{L,R}_{Z\chi^{\pm\pm}\chi^{\mp\mp}}=-\frac{1}{e}C^{L,R}_{Z\chi^{\pm\pm}\chi^{\mp\mp}}.$$

As discussed in Ref. [25], the QCD corrections to the process $h\to Z\gamma$ are approximately 0.1%, which indicates that the QCD corrections can be neglected safely. In other words, we can safely neglect the QCD corrections because they are very small.

Compared to the indirect contributions, the direct contributions are very different, and they can be calculated in a power series $(m_q/m_h)^2$ or $(\Lambda_{\rm QCD}/m_h)^2$. For the transversely polarized vector meson, the leading-twist projections provide direct contributions. We can obtain the direct contributions by the asymptotic function $\phi_M^{\perp}=6x(1-x)$ [26–28].

$$F^{MZ}_{\perp\rm direct}=\sum_q f_M^{q\perp}v_q\kappa_q\frac{3m_q}{2m_M}\frac{1-r_Z^2+2r_Z\ln r_Z}{(1-r_Z)^2},\tag{16}$$

$$\tilde{F}^{MZ}_{\perp\rm direct}=\sum_q f_M^{q\perp}v_q\tilde{\kappa}_q\frac{3m_q}{2m_M}\frac{1-r_Z^2+2r_Z\ln r_Z}{(1-r_Z)^2}.\tag{17}$$

In the calculations, it is found that the direct contribution is much smaller than the indirect contribution. This indicates that the indirect contributions are more important than the direct contributions. The contributions for the

decay width of $h \to MZ$ in the SM are presented in Table 2.

Normalized to the SM expectation, the signal strengths for the Higgs decay channels can be quantified as

$$\mu_{MZ}^{ggF} = \frac{\sigma_{\rm NP}(ggF)Br_{\rm NP}(h \to MZ)}{\sigma_{\rm SM}(ggF)Br_{\rm SM}(h \to MZ)}, \tag{18}$$

$$\mu_{\gamma\gamma}^{ggF} = \frac{\sigma_{\rm NP}(ggF)Br_{\rm NP}(h \to \gamma\gamma)}{\sigma_{\rm SM}(ggF)Br_{\rm SM}(h \to \gamma\gamma)}, \tag{19}$$

where ggF stands for gluon-gluon fusion. The Higgs production cross sections can be written as

$$\frac{\sigma_{\rm NP}(ggF)}{\sigma_{\rm SM}(ggF)} \approx \frac{\Gamma_{\rm NP}(h \to gg)}{\Gamma_{\rm SM}(h \to gg)}. \tag{20}$$

Through Eqs. (18)–(20), the signal strengths for $h \to MZ$ and $h \to \gamma\gamma$ can be quantified as

$$\begin{aligned}\mu_{MZ}^{ggF} &\approx \frac{\Gamma_{\rm NP}(h \to gg)\Gamma_{\rm NP}(h \to MZ)/\Gamma_{\rm NP}^{h}}{\Gamma_{\rm SM}(h \to gg)\Gamma_{\rm SM}(h \to MZ)/\Gamma_{\rm SM}^{h}} \\ &= \frac{\Gamma_{\rm NP}(h \to gg)\Gamma_{\rm NP}(h \to MZ)\Gamma_{\rm SM}^{h}}{\Gamma_{\rm SM}(h \to gg)\Gamma_{\rm SM}(h \to MZ)\Gamma_{\rm NP}^{h}},\end{aligned} \tag{21}$$

$$\begin{aligned}\mu_{\gamma\gamma}^{ggF} &\approx \frac{\Gamma_{\rm NP}(h \to gg)\Gamma_{\rm NP}(h \to \gamma\gamma)/\Gamma_{\rm NP}^{h}}{\Gamma_{\rm SM}(h \to gg)\Gamma_{\rm SM}(h \to \gamma\gamma)/\Gamma_{\rm SM}^{h}} \\ &= \frac{\Gamma_{\rm NP}(h \to gg)\Gamma_{\rm NP}(h \to \gamma\gamma)\Gamma_{\rm SM}^{h}}{\Gamma_{\rm SM}(h \to gg)\Gamma_{\rm SM}(h \to \gamma\gamma)\Gamma_{\rm NP}^{h}},\end{aligned} \tag{22}$$

where $\Gamma_{\rm NP}^{h}$ and $\Gamma_{\rm SM}^{h}$ denote the total decay widths in the NP model and SM, respectively.

IV. NUMERICAL ANALYSIS

In this section, we discuss the numerical results of the Higgs boson decays $h \to MZ$ in the TNMSSM. The results are constrained by the SM-like Higgs boson mass in the TNMSSM with $124.74\,{\rm GeV} \le m_h \le 125.76\,{\rm GeV}$, where a 3σ experimental error is considered. For the SM parameters, we take $m_W = 80.385$ GeV, $m_Z = 91.1876$ GeV, $m_u = 2.16$ MeV, $m_d = 4.67$ MeV, $m_s = 93.4$ MeV, $m_c = 1.27$ GeV, $m_b = 4.18$ GeV, and $m_t = 172.69$ GeV. For the squark sector, we take $m_{\tilde{Q}} = m_{\tilde{u}} = m_{\tilde{d}} = {\rm diag}(M_Q, M_Q, M_Q)$ and $T_{u,d} = Y_{u,d}\,{\rm diag}(A_Q, A_Q, A_t)$ for simplicity. According to the latest experimental data [3], we take $M_Q = 2$ TeV and $A_Q = 1.5$ TeV, and for the slepton sector, we take $m_{\tilde{l}} = m_{\tilde{e}} = 2$ TeV, $T_e = Y_e{\rm diag}(A_e, A_e, A_e)$, and $A_e = 1.5$ TeV. Then, we take $\mu = 1$ TeV, $\tan\beta = 8$, $\tan\beta' = 10$, $\lambda = 0.95$, $\kappa = 0.9$, $\chi_t = 0.4$, $T_{\Lambda_T} = 1.5$ TeV, $T_\kappa = 700$ GeV, $T_\lambda = -700$ GeV, and $\sqrt{v_T^2 + \bar{v}_T^2} = 2$ GeV. We employ the following parameters as variable parameters in the numerical analysis:

$$M_2,\ \Lambda_T,\ \chi_d,\ A_t,\ T_{\chi_t},\ T_{\chi_d}.$$

In our next numerical analysis, the lightest chargino is always of more than 800 GeV, and the masses of sleptons and squarks are all of more than 1900 GeV.

A. $h \to \gamma\gamma$, $h \to VV^*$, and $h \to Z\gamma$ in the TNMSSM

In this subsection, we calculate the signal strengths for the $h \to \gamma\gamma$, $h \to VV^*$, and $h \to Z\gamma$processes. Some relevant formulas of $h \to \gamma\gamma$ and $h \to VV^*$ can be found in [23, 24]. First, we take the parameters $M_2 = 1500$ GeV, $\Lambda_T = 0.8$, $A_t = 1500$ GeV, and $T_{\chi_d} = -800$ GeV. The signal strength of $h \to \gamma\gamma$ varying with χ_d is depicted in Fig. 3(a) for $T_{\chi_t} = -800$ GeV (solid line), $T_{\chi_t} = -900$ GeV (dashed line), and $T_{\chi_t} = -1000$ GeV (dot dashed line). The SM-like Higgs mass should satisfy the 3σ error of experimental constraints, and thus, we let χ_d vary from 0.5 to 1. In Fig. 3(a), all the three curves are $1.03 < \mu_{\gamma\gamma}^{ggF} < 1.16$ and they behave in a similar manner. These curves tend to decrease with the increase in χ_d. The solid line varies from 1.16 to 1.05, the dashed line varies from 1.15 to 1.045, and the dot dashed line varies from 1.14 to 1.035. Our results for the $h \to \gamma\gamma$ process satisfy the experiment constraints [3].

The signal strengths for the processes $h \to ZZ^*$ and $h \to WW^*$ are very close. Therefore, we take $\mu_{VV^*}^{ggF} = \mu_{WW^*}^{ggF} = \mu_{ZZ^*}^{ggF}$ for simplicity, and we only show the signal strength of $h \to ZZ^*$. We take the parameters $M_2 = 1500$ GeV, $T_{\chi_d} = -800$ GeV, $T_{\chi_t} = -800$ GeV, and $A_t = 1500$ GeV, and we display the signal strength of $h \to VV^*$ varying with χ_d in Fig. 3(b) for $\Lambda_T = 0.7$ (solid line), $\Lambda_T = 0.8$ (dashed line), and $\Lambda_T = 0.9$ (dot dashed line). In Fig. 3(b), the signal strength of $h \to VV^*$ decreases with the increase in χ_d. These curves are above 1.073 and below 1.171, and their behaviors are similar. The experiment constraints [3] are $\mu_{ZZ^*}^{(\rm exp)} = 1.01 \pm 0.07$,

Table 2. Contributions for the decay width of $h \to MZ$ in the SM, with $C_{\gamma Z}^{\rm SM} \simeq -2.43$.

	ρ	ω	ϕ	J/ψ	Y
$F_{\parallel{\rm ind}}^{MZ}$	$0.0423 + 4.3\times10^{-4}C_{\gamma Z}^{\rm SM}$	$-0.0102 + 1.3\times10^{-4}C_{\gamma Z}^{\rm SM}$	$-0.0392 - 2.1\times10^{-4}C_{\gamma Z}^{\rm SM}$	$0.041 + 7.5\times10^{-4}C_{\gamma Z}^{\rm SM}$	$-0.115 - 6.1\times10^{-4}C_{\gamma Z}^{\rm SM}$
$F_{\perp{\rm ind}}^{MZ}$	$0.042 + 1.181C_{\gamma Z}^{\rm SM}$	$-0.01 + 0.343C_{\gamma Z}^{\rm SM}$	$-0.039 - 0.327C_{\gamma Z}^{\rm SM}$	$0.04 + 0.128C_{\gamma Z}^{\rm SM}$	$-0.12 - 0.011C_{\gamma Z}^{\rm SM}$
$F_{\perp{\rm direct}}^{MZ}$	0.0037	−0.00087	−0.00257	−0.00088	−0.00080

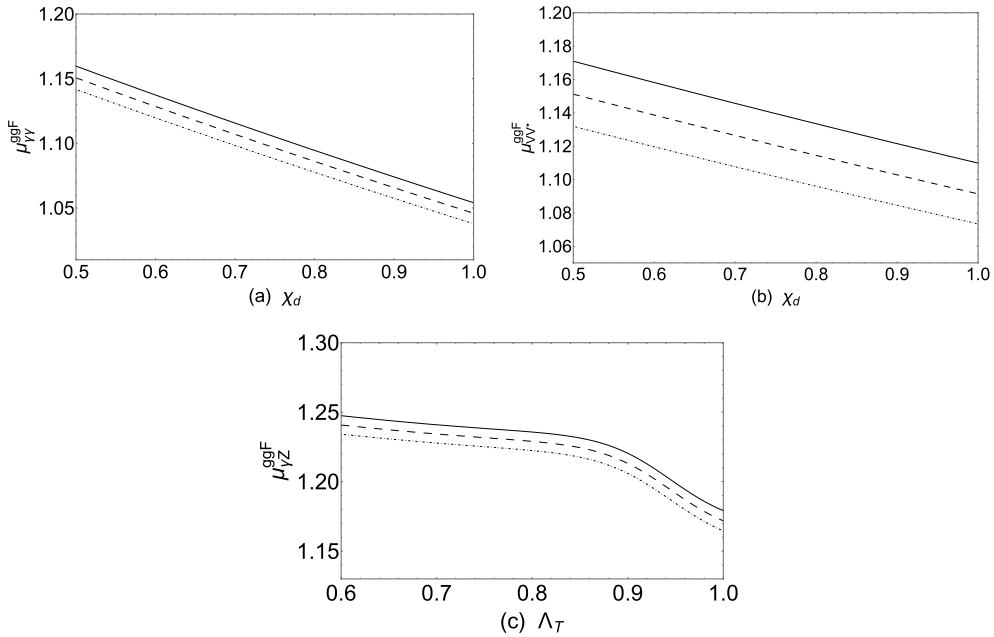

Fig. 3. (a) $\mu^{ggF}_{\gamma\gamma}$ varing with χ_d for $T_{\chi_t} = -800$ GeV (solid line), $T_{\chi_t} = -900$ GeV (dashed line), and $T_{\chi_t} = -1000$ GeV (dot dashed line). (b) $\mu^{ggF}_{VV^*}$ varying with χ_d for $\Lambda_T = 0.7$ (solid line), $\Lambda_T = 0.8$ (dashed line), and $\Lambda_T = 0.9$ (dot dashed line). (c) $\mu^{ggF}_{Z\gamma}$ varying with Λ_T for $\chi_d = 0.7$ (solid line), $\chi_d = 0.8$ (dashed line), and $\chi_d = 0.9$ (dot dashed line).

$\mu^{(\exp)}_{WW^*} = 1.19 \pm 0.12$. Thus, our calculated result $\mu^{ggF}_{ZZ^*}$ satisfies the experimental constraint where the error is 1σ, and $\mu^{ggF}_{WW^*}$ satisfies the experimental constraint where the error is 2σ.

The new physics contributions to the decay $h \to MZ$ come from the effective coupling of $hZ\gamma$. Therefore, we study the process $h \to Z\gamma$ in this subsection. In the numerical calculation of the process $h \to Z\gamma$, we take the parameters $M_2 = 1500$ GeV, $T_{\chi_d} = -800$ GeV, $T_{\chi_t} = -800$ GeV, and $A_t = 1500$ GeV. In Fig. 3(c), these curves are close to each other, and they vary from 1.164 to 1.248. When $0.6 \le \Lambda_T \le 0.9$, all the lines have a smaller slope, and when $0.9 \le \Lambda_T \le 1$, all the lines here have a larger slope. The result agrees with the observed signal strength with 1.5σ.

B. Processes $h \to MZ$

In this subsection, we will study the processes $h \to MZ$. The vector meson decay constants for ω, ρ, ϕ, J/ψ, and Y can be found in Table 1. The NP contribution of the process $h \to MZ$ comes from the effective coupling $hZ\gamma$. Thus, our calculated results of the $h \to MZ$ decay for different mesons should be similar.

Now, we study the signal strengths of the process $h \to MZ$. First, we take the parameters $T_{\chi_d} = -800$ GeV, $T_{\chi_t} = -800$ GeV, and $A_t = 1500$ GeV. We depict the signal strengths of the $h \to MZ$ processes in Fig. 4. In Fig. 4, the solid line is obtained with $\chi_d = 0.7$, $\Lambda_T = 0.9$; the dashed line is obtained with $\chi_d = 0.8$, $\Lambda_T = 0.8$; and the dot dashed line is obtained with $\chi_d = 0.9$, $\Lambda_T = 0.7$. As can be observed from Fig. 4, the signal strengths increase with the increase in M_2 at 1000 GeV $\le M_2 \le$ 1100 GeV, and the signal strengths decrease with the increase in M_2 at 1100 GeV $\le M_2 \le$ 2000 GeV. The signal strengths of the $h \to \omega Z$ processes are in the 1.18–1.223 region; the signal strengths of the $h \to \rho Z$ processes are in the 1.183–1.235 region; the signal strengths of the $h \to \phi Z$ processes are in the 1.141–1.172 region; the signal strengths of the $h \to J\psi Z$ processes are in the 1.147–1.179 region; and the signal strengths of the $h \to \Upsilon Z$ processes are in the 1.108–1.138 region.

The new contributions to the $h \to MZ$ decay come from the effective coupling of $h\gamma Z$. Thus, we can infer that our results are consistent with the $h \to \gamma Z$ process. As can be observed in Fig. 3(c), the parameter Λ_T has obvious influence on the signal strength $\mu^{ggF}_{Z\gamma}$. Thereore, we should research the signal strengths of the $h \to MZ$ processes versus Λ_T. We take the parameters $M_2 = 1500$ GeV, $T_{\chi_d} = -800$ GeV, $T_{\chi_d} = -800$ GeV, and $A_t = 1500$ GeV. The Higgs mass should satisfy the 3σ error of the experimental constraints, and hence, Λ_T is changed from 0.6 to 1 with $\chi_d = 0.7, 0.8, 0.9$. The results for signal strengths of μ^{ggF}_{MZ} versus Λ_T are plotted in Fig. 5. The $\mu^{ggF}_{\omega Z}$ values are in the 1.133–1.238 region, the $\mu^{ggF}_{\rho Z}$ values are in the 1.138–1.249 region, the $\mu^{ggF}_{\phi Z}$ values are in the 1.109–1.191 region, the $\mu^{ggF}_{J/\psi Z}$ values are in the 1.112–1.198 region, and the $\mu^{ggF}_{\Upsilon Z}$ values are in the 1.07–1.155 region. It can be observed that the signal strengths of $h \to MZ$ are similar to the signal strength of $h \to Z\gamma$. In Fig. 5, with solid lines, all the curves vary from 1.164 to

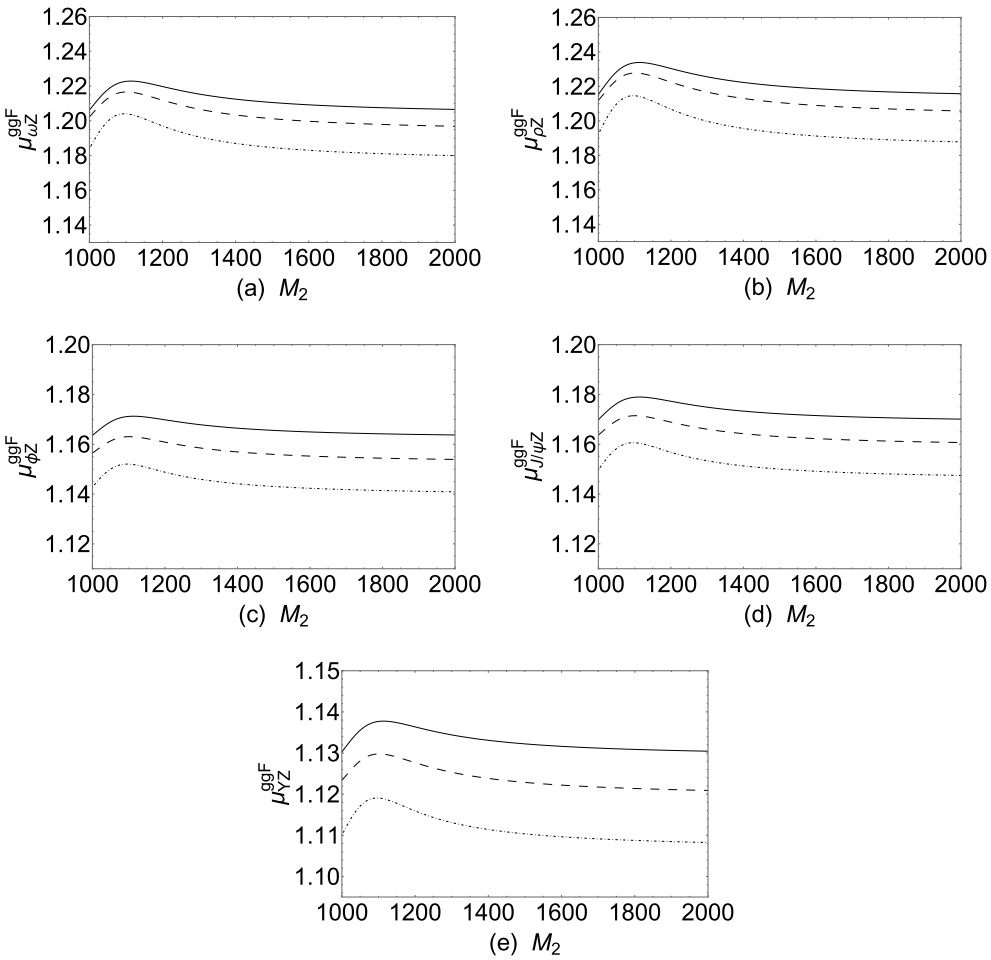

Fig. 4. Signal strengths versus M_2 for $\chi_d = 0.7$, $\Lambda_T = 0.9$ (solid line), $\chi_d = 0.8$, $\Lambda_T = 0.8$ (dashed line), and $\chi_d = 0.9$, $\Lambda_T = 0.7$ (dot dashed line).

1.248. When $0.6 \leq \Lambda_T \leq 0.9$, all the lines here have a smaller slope. When $0.9 \leq \Lambda_T \leq 1$, all the lines here have a larger slope. As can be observed, the signal strengths of $h \to MZ$ decrease as χ_d increases.

We now study the effect of T_{χ_d} on the signal strengths of $h \to MZ$. We take the parameters $M_2 = 1500$ GeV, $\Lambda_T = 0.8$, $\chi_d = 0.7$, and $T_{\chi_t} = -800$ GeV. The SM-like Higgs mass should satisfy the 3σ error of the experimental constraints, and thus, we let T_{χ_d} vary from -1000 GeV to 1000 GeV with $A_t = 1000$, 1200, 1500 GeV. We plot the signal strengths of the $h \to MZ$ processes in Fig. 6. In Fig. 6, the solid lines are obtained with $A_t = 1000$ GeV, the dashed lines are obtained with $A_t = 1200$ GeV, and the dot dashed lines are obtained with $A_t = 1500$ GeV. In Fig. 6, we can see that the signal strengths increase with the increase in T_{χ_d} . In Fig. 6(a) and Fig. 6(b), the signal strengths of the $h \to \omega Z$ and $h \to \rho Z$ processes are in the 1.181–1.227 and 1.19–1.237 regions, respectively. In Fig. 6(c) and Fig. 6(d), the signal strengths of the $h \to \phi Z$ and $h \to J/\psi Z$ processes are in the 1.138–1.178 and 1.145–1.186 regions, respectively. The meson Y is the heaviest meson we have studied, and thus, the signal strength of the $h \to \Upsilon Z$ process is obviously lower than the other results in Fig. 6. The signal strength of the $h \to \Upsilon Z$ process is in the 1.105–1.142 region. We can see from Fig. 6 that A_t has a great influence on the signal strengths of $h \to MZ$. The signal strengths of $h \to MZ$ increase as A_t increases.

Finally, we study the effect of A_t on the signal strengths of the $h \to MZ$processes. The coupling of Higgs and third generation squarks include A_t. We take the parameters $M_2 = 1500$ GeV, $T_{\chi_d} = -800$ GeV, and $T_{\chi_t} = -800$ GeV. The SM-like Higgs mass should satisfy the 3σ error of the experimental constrains, and thus, we let A_t vary from -1000 GeV to 1000 GeV with $(\Lambda_T = 0.5, \chi_d = 0.8)$, $(\Lambda_T = 0.6, \chi_d = 0.7)$, and $(\Lambda_T = 0.7, \chi_d = 0.6)$. We plot the signal strengths of the $h \to MZ$ process in Fig. 7. In Fig. 7, the solid lines are obtained with $\Lambda_T = 0.5$, $\chi_d = 0.8$, the dashed lines are obtained with $\Lambda_T = 0.6$, $\chi_d = 0.7$, and the dot dashed lines are obtained with $\Lambda_T = 0.7$, $\chi_d = 0.6$. In Fig. 7(a) and Fig. 7(b), the signal strengths of the $h \to \omega Z$ and $h \to \rho Z$ processes are in

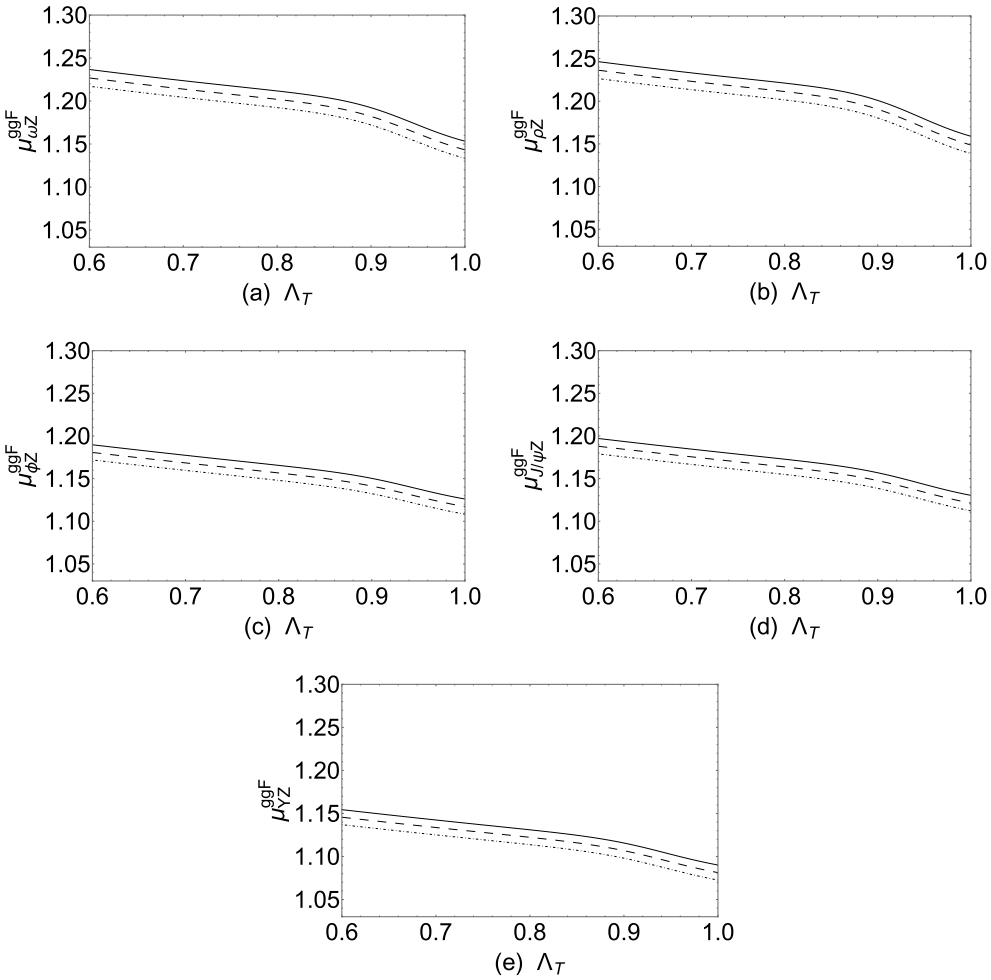

Fig. 5. Signal strengths versus Λ_T plotted with a solid line ($\chi_d = 0.7$), dashed line ($\chi_d = 0.8$), and dot dashed line ($\chi_d = 0.9$).

the 1.165–1.253 and 1.174–1.265 regions, respectively. The signal strengths of the $h \to \phi Z$ and $h \to J/\psi Z$ processes are in the 1.125–1.205 and 1.132–1.213 regions. For the heaviest meson Y we have studied, the signal strength of $h \to \Upsilon Z$ is obviously lower than the other results in Fig. 7. The lines in Fig. 7(e) are in the 1.095–1.169 region.

V. CONCLUSION

In this work, we study the decays $h \to \gamma Z$ and $h \to MZ$ in the TNMSSM, with $M = \omega, \rho, \phi, J/\psi, \Upsilon$. The $h \to MZ$ decay has two types of contributions: direct and indirect. For the indirect contributions, there is a process $h \to Z\gamma^* \to MZ$, where γ^* is off-shell and changes into the final state vector meson. No $h\gamma Z$ coupling exists at the tree level, but it can be contributed by a loop diagram. In the models beyond the SM, the coupling constant can be divided into two parts: *CP*-even coupling constant $C_{\gamma Z}$ and *CP*-odd coupling constant $\tilde{C}_{\gamma Z}$. The *CP*-even coupling constant $C_{\gamma Z}$ is more important than the *CP*-odd coupling constant $\tilde{C}_{\gamma Z}$.

The experiment results of the signal strengths $\mu^{ggF}_{\gamma\gamma}$ and μ^{ggF}_{ZZ} are $\mu^{ggF}_{\gamma\gamma} = 1.10 \pm 0.07$ and $\mu^{ggF}_{ZZ} = 1.01 \pm 0.07$. Our numerical results of the signal strengths $\mu^{ggF}_{\gamma\gamma}$ and μ^{ggF}_{ZZ} are in the 1.035–1.16 and 1.073–1.171 regions, which satisfy the error of 1σ. Our numerical results of the signal strength in the 1.164–1.248 region agree with the observed signal strength with 1.5σ. The numerical results show that the TNMSSM contributions to the $h \to \omega Z$ and $h \to \rho Z$ processes are more significant. The signal strengths $\mu^{ggF}_{\omega Z, \rho Z}$ are approximately 1.13–1.26. The TNMSSM corrections to the $h \to \phi Z$ and $h \to J/\psi Z$ processes are 1.11–1.21, and to $h \to \Upsilon Z$ they are approximately 1.07–1.17. The $h \to MZ$ decays may be accessible at future high energy colliders.

APPENDIX A: FORM FACTORS

The form factors are

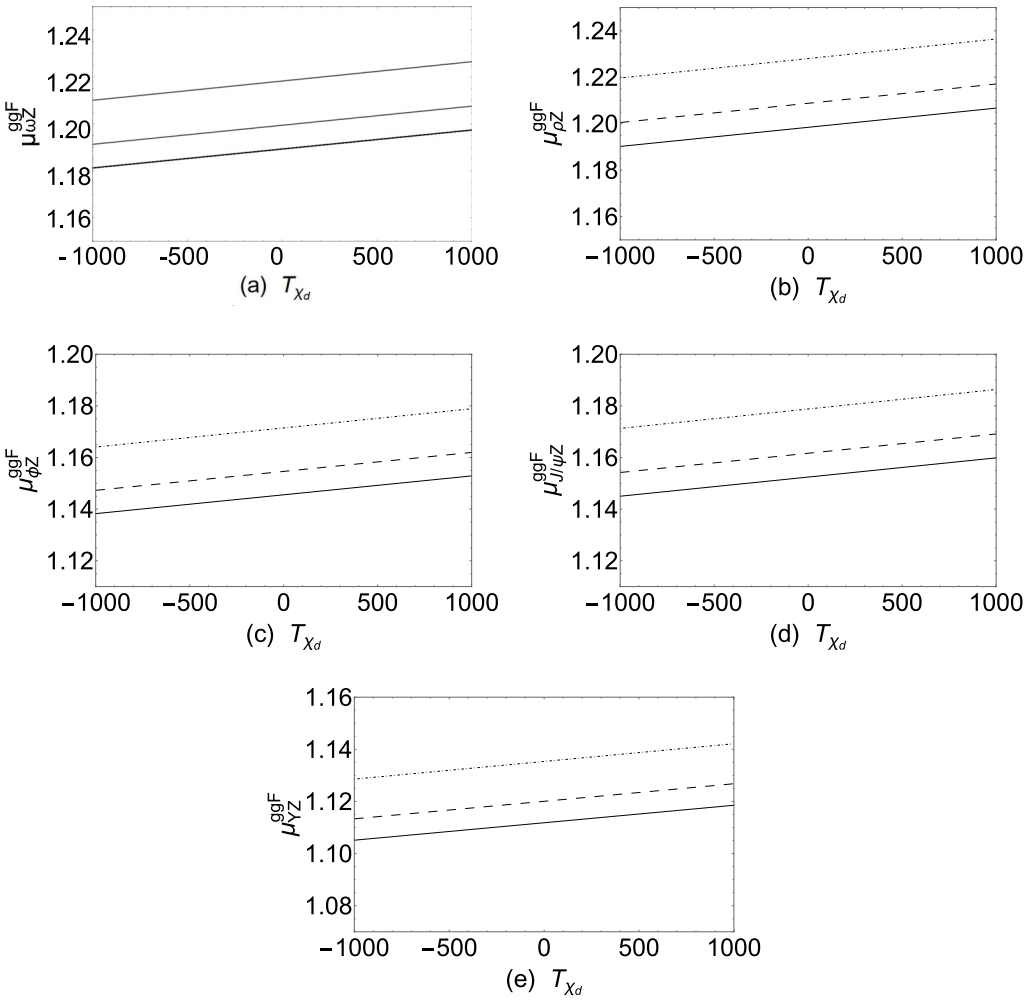

Fig. 6. Signal strengths versus T_{χ_d} plotted for $A_t = 1000\,\text{GeV}$ (solid line), $A_t = 1200\,\text{GeV}$ (dashed line), and $A_t = 1500\,\text{GeV}$ (dot dashed line).

$$A_0(\tau,\lambda) = I_1(\tau,\lambda), \tag{A1}$$

$$A_{1/2}(\tau,\lambda) = I_1(\tau,\lambda) - I_2(\tau,\lambda) \tag{A2}$$

with

$$I_1(\tau,\lambda) = \frac{\tau\lambda}{2(\tau-\lambda)} + \frac{\tau^2\lambda^2}{2(\tau-\lambda)^2}[f(\tau^{-1}) - f(\lambda^{-1})] + \frac{\tau^2\lambda}{(\tau-\lambda)^2}[g(\tau^{-1}) - g(\lambda^{-1})], \tag{A3}$$

$$I_2(\tau,\lambda) = -\frac{\tau\lambda}{2(\tau-\lambda)}[f(\tau^{-1}) - f(\lambda^{-1})]. \tag{A4}$$

Here, $f(x)$ and $g(x)$ are as follows:

$$f(x) = \begin{cases} \arcsin^2\sqrt{x}, & x \le 1 \\ -\dfrac{1}{4}\left[\ln\dfrac{1+\sqrt{1-1/x}}{1-\sqrt{1-1/x}} - \mathrm{i}\pi\right]^2, & x > 1 \end{cases} \tag{A5}$$

$$g(x) = \begin{cases} \sqrt{x^{-1}-1}\arcsin\sqrt{x}, & x \ge 1 \\ \dfrac{\sqrt{1-x^{-1}}}{2}\left[\ln\dfrac{1+\sqrt{1-1/x}}{1-\sqrt{1-1/x}} - \mathrm{i}\pi\right], & x < 1 \end{cases} \tag{A6}$$

APPENDIX B: MASS OF HIGGS AND CHARGINOS

In the basis $(\phi_d, \phi_u, \phi_s, \phi_T, \phi_{\bar{T}})$, the definition of mass squared matrix for neutral Higgs is given by

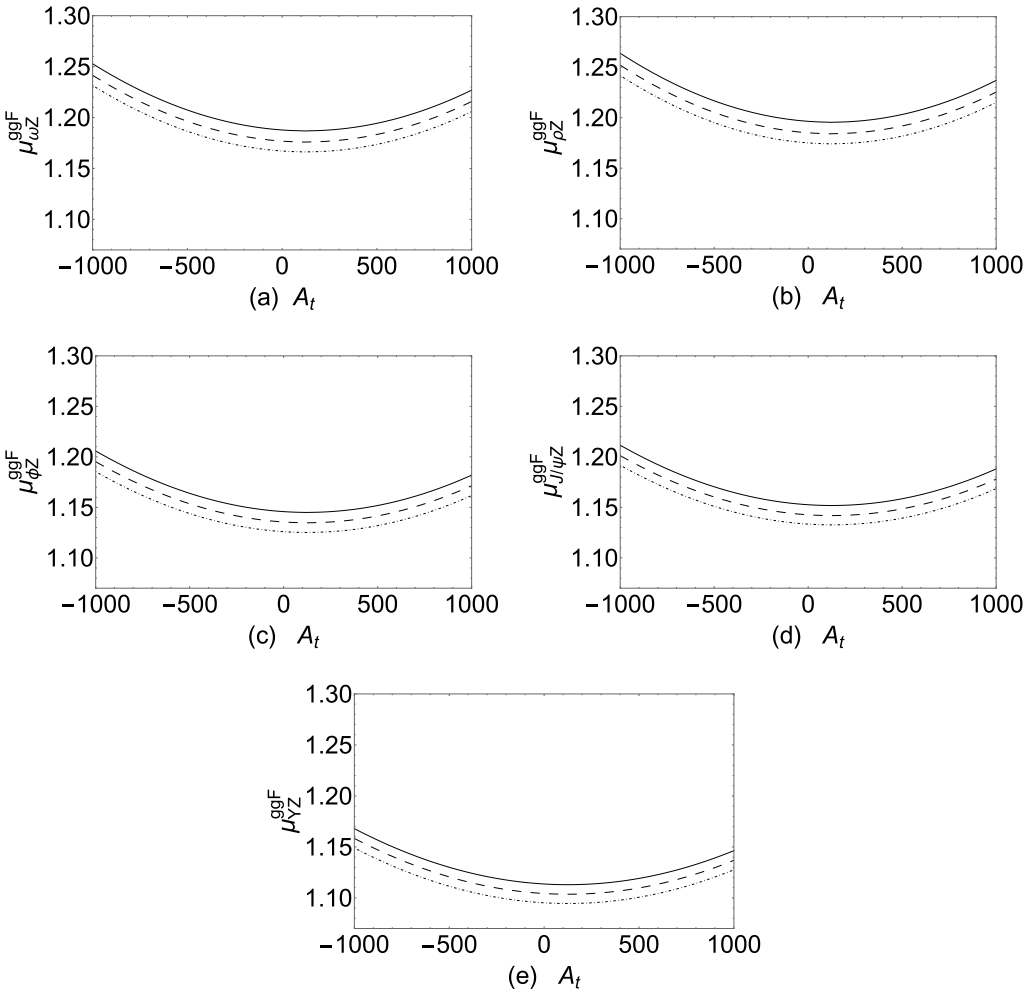

Fig. 7. Signal strengths versus A_t plotted for $\Lambda_T = 0.5$, $\chi_d = 0.8$ (solid line), $\Lambda_T = 0.6$, $\chi_d = 0.7$ (dashed line), and $\Lambda_T = 0.7$, $\chi_d = 0.6$ (dot dashed line).

$$m_h^2 = \begin{pmatrix} m_{\phi_d\phi_d} & m_{\phi_u\phi_d} & m_{\phi_s\phi_d} & m_{\phi_T\phi_d} & m_{\phi_{\bar{T}}\phi_d} \\ m_{\phi_d\phi_u} & m_{\phi_u\phi_u} & m_{\phi_s\phi_u} & m_{\phi_T\phi_u} & m_{\phi_{\bar{T}}\phi_u} \\ m_{\phi_d\phi_s} & m_{\phi_u\phi_s} & m_{\phi_s\phi_s} & m_{\phi_T\phi_s} & m_{\phi_{\bar{T}}\phi_s} \\ m_{\phi_d\phi_T} & m_{\phi_u\phi_T} & m_{\phi_s\phi_T} & m_{\phi_T\phi_T} & m_{\phi_{\bar{T}}\phi_T} \\ m_{\phi_d\phi_{\bar{T}}} & m_{\phi_u\phi_{\bar{T}}} & m_{\phi_s\phi_{\bar{T}}} & m_{\phi_T\phi_{\bar{T}}} & m_{\phi_{\bar{T}}\phi_{\bar{T}}} \end{pmatrix} \tag{B1}$$

where

$$\begin{aligned} m_{\phi_d\phi_d} = {} & m_{H_d}^2 + \frac{1}{8}(g_1^2+g_2^2)(2v_{\bar{T}}^2 - 2v_T^2 + 3v_d^2 - v_u^2) \\ & + \sqrt{2}v_T\Re(T_{\chi_d}) + \frac{|\lambda|^2}{2}(v_s^2+v_u^2) \\ & - v_s v_{\bar{T}}\Re(\chi_d\Lambda_T^*) + (3v_d^2+2v_T^2)|\chi_d|^2, \end{aligned} \tag{B2}$$

$$\begin{aligned} m_{\phi_d\phi_u} = {} & -\frac{1}{4}(g_1^2+g_2^2)v_d v_u - \frac{1}{\sqrt{2}}v_s\Re(T_\lambda) \\ & + \frac{1}{2}v_T v_{\bar{T}}\Re(\lambda\Lambda_T^*) + v_d v_u|\lambda|^2 - v_s v_{\bar{T}}\Re(\chi_t\lambda^*) \\ & - v_s v_T\Re(\chi_d\lambda^*) - \frac{1}{2}v_s^2\Re(\kappa\lambda^*), \end{aligned} \tag{B3}$$

$$\begin{aligned} m_{\phi_u\phi_u} = {} & m_{H_u}^2 - \frac{1}{8}(g_1^2+g_2^2)(2v_{\bar{T}}^2 - 2v_T^2 - 3v_u^2 + v_d^2) \\ & + \sqrt{2}v_{\bar{T}}\Re(T_{\chi_t}) + \frac{1}{2}(v_d^2+v_s^2)|\lambda|^2 \\ & - v_s v_T\Re(\chi_t\Lambda_T^*) + (2v_{\bar{T}}^2+3v_u^2)|\chi_t|^2, \end{aligned} \tag{B4}$$

$$\begin{aligned} m_{\phi_d\phi_s} = {} & v_d v_s|\lambda|^2 - \frac{1}{\sqrt{2}}v_u\Re(T_\lambda) - v_s v_u\Re(\kappa\lambda^*) \\ & - v_T v_u\Re(\lambda\chi_d^*) - v_{\bar{T}} v_u\Re(\chi_t\lambda^*) - v_d v_{\bar{T}}\Re(\Lambda_T\chi_d^*), \end{aligned} \tag{B5}$$

$$m_{\phi_u\phi_s} = v_s v_u|\lambda|^2 - \frac{1}{\sqrt{2}}v_d\Re(T_\lambda) - v_d v_s\Re(\lambda\kappa^*) - v_T v_d\Re(\lambda\chi_d^*) - v_d v_{\bar{T}}\Re(\lambda\chi_t^*) - v_T v_u\Re(\chi_t\Lambda_T^*), \tag{B6}$$

$$m_{\phi_s\phi_s} = m_S^2 + \frac{|\Lambda_T|^2}{2}(v_T^2+v_{\bar{T}}^2) - v_T v_{\bar{T}}\Re(\kappa\Lambda_T^*) + 3v_s^2|\kappa|^2 - v_d v_u\Re(\lambda\kappa^*) + \frac{1}{2}(v_d^2+v_u^2)|\lambda|^2, + \sqrt{2}v_s\Re(T_\kappa), \tag{B7}$$

$$m_{\phi_d\phi_T} = -\frac{1}{2}(g_1^2+g_2^2)v_d v_u + \frac{1}{2}v_u v_{\bar{T}}\Re(\lambda\Lambda_T^*) - v_u v_s\Re(\lambda\chi_d^*) + 4v_d v_T|\chi_d|^2 + \sqrt{2}v_d\Re(T_{\chi_d}), \tag{B8}$$

$$m_{\phi_u\phi_T} = \frac{1}{2}(g_1^2+g_2^2)v_d v_T - v_u v_s\Re(\Lambda_T\chi_t^*) - v_d v_s\Re(\lambda\chi_d^*) + \frac{1}{2}v_d v_{\bar{T}}\Re(\lambda\Lambda_T^*), \tag{B9}$$

$$m_{\phi_s\phi_T} = v_s v_T|\lambda|^2 - \frac{1}{\sqrt{2}}v_{\bar{T}}\Re(T_\Lambda) - v_s v_{\bar{T}}\Re(\kappa\Lambda_T^*) - v_d v_u\Re(\lambda\chi_d^*) - \frac{1}{2}v_u^2\Re(\chi_t\Lambda_T^*), \tag{B10}$$

$$m_{\phi_T,\phi_T} = m_T^2 - \frac{1}{4}(g_1^2+g_2^2)(2v_{\bar{T}}^2 - 6v_T^2 - v_u^2 + v_d^2) + 2v_d^2|\chi_d|^2 + \frac{1}{2}(v_s^2+v_{\bar{T}}^2)|\Lambda_T|^2, \tag{B11}$$

$$m_{\phi_d,\phi_{\bar{T}}} = \frac{1}{2}(g_1^2+g_2^2)v_d v_{\bar{T}} + \frac{1}{2}v_T v_u\Re(\lambda\Lambda_T^*) - v_d v_s\Re(\chi_d\Lambda_T^*) - v_s v_u\Re(\chi_t\lambda^*), \tag{B12}$$

$$m_{\phi_u,\phi_{\bar{T}}} = -\frac{1}{2}(g_1^2+g_2^2)v_{\bar{T}}v_u + \sqrt{2}v_u\Re(T_{\chi_t}) + \frac{1}{2}v_d v_T\Re(\lambda\Lambda_T^*) - v_d v_s\Re(\lambda\chi_t^*) + 4v_{\bar{T}}v_u|\chi_t|^2, \tag{B13}$$

$$m_{\phi_s,\phi_T} = v_s v_{\bar{T}}|\Lambda_T|^2 - \frac{1}{\sqrt{2}}v_T\Re(T_\Lambda) - v_s v_T\Re(\kappa\Lambda_T^*) - \frac{1}{2}v_d^2\Re(\Lambda_T\chi_d^*) - v_d v_u\Re(\lambda\chi_t^*), \tag{B14}$$

$$m_{\phi_T,\phi_{\bar{T}}} = -(g_1^2+g_2^2)v_T v_{\bar{T}} - \frac{1}{\sqrt{2}}v_s\Re(T_\Lambda) - \frac{1}{2}v_s^2\Re(\kappa\Lambda_T^*) + \frac{1}{2}v_d v_u\Re(\lambda\Lambda_T^*) + v_T v_{\bar{T}}|\Lambda_T|^2, \tag{B15}$$

$$m_{\phi_{\bar{T}},\phi_{\bar{T}}} = m_{\bar{T}}^2 + \frac{1}{4}(g_1^2+g_2^2)(v_d^2 - v_u^2 - 2v_T^2 + 6v_{\bar{T}}) + \frac{1}{2}(v_s^2+v_T^2)|\Lambda_T|^2 + 2v_u^2|\chi_t|^2. \tag{B16}$$

This matrix is diagonalized by $Z^{\rm H}$:

$$Z^{\rm H}m_h^2 Z^{\rm H,\dagger} = m_{2,h}^{\rm dia}$$

with

$$\phi_d = \sum_j Z_{j1}^{\rm H}h_j,\ \ \phi_u = \sum_j Z_{j2}^{\rm H}h_j,\ \ \phi_s = \sum_j Z_{j3}^{\rm H}h_j,$$

$$\phi_T = \sum_j Z_{j4}^{\rm H}h_j,\ \ \phi_{\bar{T}} = \sum_j Z_{j5}^{\rm H}.$$

In the basis $(\tilde{W}^-,\tilde{H}_d^-,\tilde{T}^-)$, $(\tilde{W}^+,\tilde{H}_u^+,\tilde{T}^+)$, the definition of mass matrix for charginos is given by

$$m_{\tilde{\chi}^-} = \begin{pmatrix} M_2 & \frac{1}{\sqrt{2}}g_2 v_u & g_2 v_T \\ \frac{1}{\sqrt{2}}g_2 v_d & \frac{1}{\sqrt{2}}v_s\lambda & -v_d\chi_d \\ g_2 v_{\bar{T}} & -v_u\chi_t & \frac{1}{\sqrt{2}}\Lambda_T v_s \end{pmatrix} \tag{B17}$$

This matrix is diagonalized by U and V

$$U^* m_{\tilde{\chi}^-} V^\dagger = m_{\tilde{\chi}^-}^{dia}$$

with

$$\tilde{W}^- = \sum_j U_{j1}^*\lambda_j^-,\quad \tilde{H}_d^- = \sum_j U_{j2}^*\lambda_j^-,\quad \tilde{T}^- = \sum_j U_{j3}^*\lambda_j^-$$
$$\tilde{W}^+ = \sum_j V_{1j}^*\lambda_j^+,\quad \tilde{H}_u^+ = \sum_j V_{2j}^*\lambda_j^+,\quad \tilde{T}^+ = \sum_j V_{3j}^*\lambda_j^+$$

APPENDIX C: TADPOLE EQUATION AND SOME CORRESPONDING VERTEXES

The *CP*-even tree level part of the tadpole are given by

$$\begin{aligned}\frac{\partial V}{\partial \phi_d} =& +\frac{1}{8}\left(g_1^2+g_2^2\right)v_d\left(2v_{\bar{T}}^2-2v_T^2-v_u^2+v_d^2\right)+\frac{1}{4}\Big(v_{\bar{T}}\Big(\Big(-2v_dv_s\chi_d+v_Tv_u\lambda\Big)\Lambda_T^*\\&-2v_sv_u\lambda\chi_t^*\Big)-v_s^2v_u\lambda\kappa^*+\Big(2v_d\left(v_s^2+v_u^2\right)\lambda+v_u\left(\Lambda_Tv_Tv_{\bar{T}}-v_s\left(2\left(v_{\bar{T}}\chi_t+v_T\chi_d\right)+v_s\kappa\right)\right)\Big)\lambda^*\\&+4v_d\Big(\sqrt{2}v_T\Re\left(T_{\chi_d}\right)+m_{H_d}^2\Big)-2\Big(\sqrt{2}v_sv_u\Re\left(T_\lambda\right)+\Big(v_d\Big(-2\left(2v_T^2+v_d^2\right)\chi_d+\Lambda_Tv_sv_{\bar{T}}\Big)+v_sv_Tv_u\lambda\Big)\chi_d^*\Big)\Big)\end{aligned}\tag{C1}$$

$$\begin{aligned}\frac{\partial V}{\partial \phi_u} =& +\frac{1}{8}\left(g_1^2+g_2^2\right)v_u\Big(-2v_{\bar{T}}^2+2v_T^2-v_d^2+v_u^2\Big)+\frac{1}{4}\Big(\Big(4v_u^3+8v_{\bar{T}}^2v_u\Big)|\chi_t|^2+v_T\Big(-2v_dv_s\lambda\chi_d^*+\Big(-2v_sv_u\chi_t+v_dv_{\bar{T}}\lambda\Big)\Lambda_T^*\Big)\\&+\Big(2\left(v_d^2+v_s^2\right)v_u\lambda+v_d\left(\Lambda_Tv_Tv_{\bar{T}}-v_s\left(2\left(v_{\bar{T}}\chi_t+v_T\chi_d\right)+v_s\kappa\right)\right)\Big)\lambda^*\\&+v_u\Big(-2\Lambda_Tv_sv_T\chi_t^*+4\Big(\sqrt{2}v_{\bar{T}}\Re\left(T_{\chi_t}\right)+m_{H_u}^2\Big)\Big)\\&+v_d\Big(-2\sqrt{2}v_s\Re\left(T_\lambda\right)+\lambda\Big(-2v_sv_{\bar{T}}\chi_t^*-v_s^2\kappa^*\Big)\Big)\Big)\end{aligned}\tag{C2}$$

$$\begin{aligned}\frac{\partial V}{\partial \phi_s} =& \frac{1}{4}\Big(\Big(-v_d^2v_{\bar{T}}\chi_d+v_s\left(2\Lambda_T\left(v_T^2+v_{\bar{T}}^2\right)-2v_Tv_{\bar{T}}\kappa\right)-v_Tv_u^2\chi_t\Big)\Lambda_T^*+\Big(-2v_dv_Tv_u\lambda-\Lambda_Tv_d^2v_{\bar{T}}\Big)\chi_d^*\\&+\Big(-2v_dv_{\bar{T}}v_u\lambda-\Lambda_Tv_Tv_u^2\Big)\chi_t^*+\Big(-2v_dv_sv_u\lambda+4v_s^3\kappa\Big)\kappa^*+v_s\Big(-2\Lambda_Tv_Tv_{\bar{T}}\kappa^*+4m_S^2\Big)\\&+2\Big(-v_dv_u\Big(v_{\bar{T}}\chi_t+v_s\kappa+v_T\chi_d\Big)+v_s\left(v_d^2+v_u^2\right)\lambda\Big)\lambda^*\\&+\sqrt{2}\Big(-2v_dv_u\Re\left(T_\lambda\right)-2v_Tv_{\bar{T}}\Re\left(T_{\Lambda_T}\right)+v_s^2\left(T_\kappa^*+T_\kappa\right)\Big)\Big)\end{aligned}\tag{C3}$$

$$\begin{aligned}\frac{\partial V}{\partial \phi_T} =& +\frac{1}{4}\left(g_1^2+g_2^2\right)v_T\Big(-2v_{\bar{T}}^2+2v_T^2-v_d^2+v_u^2\Big)+\frac{1}{4}\Big(4m_T^2v_T+\Big(2\Lambda_Tv_T\left(v_s^2+v_{\bar{T}}^2\right)+v_dv_{\bar{T}}v_u\lambda-v_s\left(v_sv_{\bar{T}}\kappa+v_u^2\chi_t\right)\Big)\Lambda_T^*\\&+\Lambda_T\Big(-v_s^2v_{\bar{T}}\kappa^*-v_sv_u^2\chi_t^*\Big)+v_d\Big(2\Big(4v_dv_T\chi_d-v_sv_u\lambda\Big)\chi_d^*+v_u\Big(-2v_s\chi_d+\Lambda_Tv_{\bar{T}}\Big)\lambda^*\Big)\\&-2\sqrt{2}v_sv_{\bar{T}}\Re\left(T_{\Lambda_T}\right)+2\sqrt{2}v_d^2\Re\left(T_{\chi_d}\right)\Big)\end{aligned}\tag{C4}$$

$$\begin{aligned}\frac{\partial V}{\partial \phi_{\bar{T}}} =& +\frac{1}{4}\left(g_1^2+g_2^2\right)v_{\bar{T}}\left(2v_{\bar{T}}^2-2v_T^2-v_u^2+v_d^2\right)+\frac{1}{4}\Big(4v_{\bar{T}}\Big(2v_u^2|\chi_t|^2+m_{\bar{T}}^2\Big)\\&+\Big(2\Lambda_T\left(v_s^2+v_T^2\right)v_{\bar{T}}+v_dv_Tv_u\lambda-v_s\Big(v_d^2\chi_d+v_sv_T\kappa\Big)\Big)\Lambda_T^*-\Lambda_Tv_s^2v_T\kappa^*+v_dv_u\Big(-2v_s\chi_t+\Lambda_Tv_T\Big)\lambda^*\\&+v_s\Big(-2\Big(\sqrt{2}v_T\Re\left(T_{\Lambda_T}\right)+v_dv_u\lambda\chi_t^*\Big)-\Lambda_Tv_d^2\chi_d^*\Big)+\sqrt{2}v_u^2\Big(T_{\chi,t^*}+T_{\chi_t}\Big)\Big)\end{aligned}\tag{C5}$$

Then, we can identify the $m_{H_d}^2$, $m_{H_u}^2$, m_S^2, m_T^2, and $m_{\bar{T}}^2$ by the minimum conditions of the scalar potential. Here, we show some corresponding vertexes in this model. Their concrete forms are shown as

$$C_{Z\chi_i^+\chi_j^-}^L=\frac{1}{2}\left(-2g_1\sin\theta_WU_{j3}^*U_{i3}+2g_2\cos\theta_WU_{j1}^*U_{i1}+(-g_1\sin\theta_W+g_2\cos\theta_W)U_{j2}^*U_{i2}\right)\tag{C6}$$

$$C_{Z\chi_i^+\chi_j^-}^R=\frac{1}{2}\left(-2g_1\sin\theta_WV_{j3}^*V_{i3}+2g_2\cos\theta_WV_{j1}^*V_{i1}+(-g_1\sin\theta_W+g_2\cos\theta_W)V_{j2}^*V_{i2}\right)\tag{C7}$$

$$C_{Z\chi^{++}\chi^-}^L=C_{h\chi^{++}\chi^-}^R=\left(-g_1\sin\theta_W+g_2\cos\theta_W\right)\tag{C8}$$

$$C^L_{h_k\chi_i^+\chi_j^-} = -\frac{1}{2}\left[g_2U^*_{j1}(2V^*_{i3}Z^H_{k4}+\sqrt{2}V^*_{i2}Z^H_{k2})+U^*_{j2}(-2\chi_dV^*_{i3}Z^H_{k1}+\sqrt{2}g_2V^*_{i1}Z^H_{k3}+\sqrt{2}\lambda V^*_{i2}Z^H_{k3})\right.$$
$$\left.+U^*_{j3}(-2\chi_tV^*_{i2}Z^H_{k2}+2g_2V^*_{i1}Z^H_{k5}+\sqrt{2}\Lambda_TV^*_{i3}Z^H_{k3})\right] \tag{C9}$$

$$C^R_{h_k\chi_i^+\chi_j^-} = -\frac{1}{2}\left[g_2U_{i1}(2V_{j3}Z^H_{k4}+\sqrt{2}V_{j2}Z^H_{k2})+U_{i2}(-2\chi^*_dV_{j3}Z^H_{k1}+\sqrt{2}g_2V_{j1}Z^H_{k3}+\sqrt{2}\lambda^*V_{j2}Z^H_{k3})\right.$$
$$\left.+U_{i3}(-2\chi^*_tV_{j2}Z^H_{k2}+2g_2V_{j1}Z^H_{k5}+\sqrt{2}\Lambda^*_TV_{j3}Z^H_{k3})\right] \tag{C10}$$

$$C^L_{h_k\chi^{++}\chi^-} = \frac{1}{\sqrt{2}}\Lambda_TZ^H_{k3} \tag{C11}$$

$$C^R_{h_k\chi^{++}\chi^-} = \frac{1}{\sqrt{2}}\Lambda^*_TZ^H_{k3} \tag{C12}$$

As the coupling between Higgs particles and charged scalar particles is very complicated, we calculate it by computer.

$$V_{\rm scalar} = W_i^*W^i+\frac{1}{2}\sum_a g_2^2\left[H_u^\dagger\frac{\sigma^a}{2}H_u+H_d^\dagger\frac{\sigma^a}{2}H_d+Tr(T^\dagger\sigma^aT)+Tr(\bar{T}^\dagger\sigma^a\bar{T})\right]^2g_1^2\left[\frac{1}{2}H_u^\dagger H_u-\frac{1}{2}H_d^\dagger H_d+T^\dagger T\right.$$
$$\left.-\bar{T}^\dagger\bar{T}+\frac{1}{6}\tilde{Q}^\dagger\tilde{Q}-\frac{1}{2}\tilde{L}^\dagger\tilde{L}-\frac{2}{3}\tilde{u}_R^*\tilde{u}_R+\frac{1}{3}\tilde{d}_R^*\tilde{d}_R+\tilde{e}_R^*\tilde{e}_R+Tr(T^\dagger T)-Tr(\tilde{T}^\dagger\tilde{T})\right]^2+V_{\rm soft}$$

where $W_i=\dfrac{\partial W}{\partial\phi_i}$. The coefficient C is as follows:

$$C_{h_k\phi_i\phi_j} = \left.\frac{\partial^3V_{\rm scalar}}{\partial h_k\partial\phi_i\partial\phi_j}\right|_{<H^0_{d,u}>=\frac{v_{d,u}}{\sqrt{2}},<S>=\frac{v_s}{\sqrt{2}},<T>=\frac{v_T}{\sqrt{2}},<\bar{T}>=\frac{v_{\bar{T}}}{\sqrt{2}},<\text{the other fields}>=0} \tag{23}$$

where ϕ_i represents the scalar field: $H^\pm$, $H^{\pm\pm}$, $\tilde{u}_L$, $\tilde{u}_R$, $\tilde{d}_L$, $\tilde{d}_R$, $\tilde{e}_L$, and $\tilde{e}_R$.

References

[1] G. Aad *et al.* (ATLAS Collaboration), Phys. Lett. B **716**, 1 (2012)
[2] S. Chatrchyan *et al.* (CMS Collaboration), Phys. Lett. B **716**, 30 (2012)
[3] R. L. Workman *et al.* (Particle Data Group), PTEP **2022**, 083C01 (2022)
[4] S. Weinberg, Phys. Rev. D **13**, 974 (1976)
[5] L. Susskind, Phys. Rev. D **20**, 2619 (1979)
[6] U. Ellwanger and C. Hugonie, Mod. Phys. Lett. A **22**, 1581 (2007), arXiv:hep-ph/0612133[hep-ph]
[7] B. Ananthanarayan and P. N. Pandita, Phys. Lett. B **371**, 245 (1996), arXiv:hep-ph/9511415[hep-ph]
[8] B. Ananthanarayan and P. N. Pandita, Int. J. Mod. Phys. A **12**, 2321 (1997), arXiv:hep-ph/9601372[hep-ph]
[9] J. D. Mason, Phys. Rev. D **80**, 015026 (2009), arXiv:0904.4485[hep-ph]
[10] K. Agashe, A. Azatov, A. Katz *et al.*, Phys. Rev. D **84**, 115024 (2011), arXiv:1109.2842[hep-ph]
[11] J. R. Espinosa and M. Quiros, Phys. Lett. B **279**, 92 (1992)
[12] J. R. Espinosa and M. Quiros, Phys. Lett. B **302**, 51 (1993), arXiv:hep-ph/9212305[hep-ph]
[13] J. R. Espinosa and M. Quiros, Phys. Rev. Lett. **81**, 516 (1998), arXiv:hep-ph/9804235[hep-ph]
[14] M. Gonzalez-Alonso and G. Isidori, Phys. Lett. B **733**, 359 (2014), arXiv:1403.2648[hep-ph]
[15] G. Isidori, A. V. Manohar, and M. Trott, Phys. Lett. B **728**, 131 (2014), arXiv:1305.0663[hep-ph]
[16] S. Alte, M. König, and M. Neubert, JHEP **12**, 037 (2016), arXiv:1609.06310[hep-ph]
[17] S. M. Zhao, T. F. Feng, J. B. Chen *et al.*, Phys. Rev. D **97**(9), 095043 (2018), arXiv:1805.05048[hep-ph]
[18] A. L. Kagan, G. Perez, F. Petriello *et al.*, Phys. Rev. Lett. **114**(10), 101802 (2015), arXiv:1406.1722[hep-ph]
[19] G. T. Bodwin, H. S. Chung, J. H. Ee *et al.*, Phys. Rev. D

90(11), 113010 (2014), arXiv:1407.6695[hep-ph]
[20] G. Aad *et al*. (ATLAS), JHEP **10**, 013 (2021), arXiv:2104.13240[hep-ex]
[21] G. Aad *et al*. (ATLAS and CMS), Phys. Rev. Lett. **132**(2), 021803 (2024), arXiv:2309.03501[hep-ex]
[22] L. Bergstrom and G. Hulth, Nucl. Phys. B **259**, 137(1985), [Erratum: Nucl. Phys. B 276, 744 (1986)]
[23] A. Djouadi, Phys. Rept. **457**, 1 (2008), arXiv:hep-ph/0503172[hep-ph]
[24] A. Djouadi, Phys. Rept. **459**, 1 (2008), arXiv:hep-ph/0503173[hep-ph]
[25] M. Spira, A. Djouadi, and P. M. Zerwas, Phys. Lett. B **276**, 350 (1992)
[26] V. L. Chernyak and A. R. Zhitnitsky, Nucl. Phys. B **201**, 492(1982), [Erratum: Nucl. Phys. B 214, 547 (1983)]
[27] N. H. Fuchs and M. D. Scadron, Phys. Rev. D **20**, 2421 (1979)
[28] M. Beneke, G. Buchalla, M. Neubert *et al*., Nucl. Phys. B **591**, 313 (2000), arXiv:hep-ph/0006124[hep-ph]